Molecular Mechanism for H_2 Release from BH_3NH_3, Including the Catalytic Role of the Lewis Acid BH_3

Minh Tho Nguyen,*,†,‡ Vinh Son Nguyen,‡ Myrna H. Matus,† G. Gopakumar,‡ and David A. Dixon*,†

Department of Chemistry, The University of Alabama, Shelby Hall, Tuscaloosa, Alabama 35487-0336, and Department of Chemistry, University of Leuven, B-3001 Leuven, Belgium

Received: September 20, 2006; In Final Form: November 19, 2006

Electronic structure calculations using various methods, up to the coupled-cluster CCSD(T) level, in conjunction with the aug-cc-pV*n*Z basis sets with n = D, T, and Q, extrapolated to the complete basis set limit, show that the borane molecule (BH_3) can act as an efficient bifunctional acid−base catalyst in the H_2 elimination reactions of XH_nYH_n systems (X, Y = C, B, N). Such a catalyst is needed as the generation of H_2 from isoelectronic ethane and borane amine compounds proceeds with an energy barrier much higher than that of the X−Y bond energy. The asymptotic energy barrier for H_2 release is reduced from 36.4 kcal/mol in BH_3NH_3 to 6.0 kcal/mol with the presence of BH_3 relative to the molecular asymptote. The NH_3 molecule can also participate in a similar catalytic process but induces a smaller reduction of the energy barrier. The kinetics of these processes was analyzed by both transition-state and RRKM theory. The catalytic effect of BH_3 has also been probed by an analysis of the electronic densities of the transition structures using the atom-in-molecule (AIM) and electron localization function (ELF) approaches.

Introduction

There is increasing interest in the development of hydrogen-based fuel cells as an environmentally friendly power source for the transportation sector. Current critical issues with hydrogen as a fuel for use in on-board transportation system include the need for efficient chemical H_2 storage materials including release/uptake of H_2.[1] Although borane amine derivatives have been known for a number of years,[2−4] their advantages and properties have only recently received significant attention.[5−8] From accurate ab initio electronic structure theory calculations, in both the gas phase and solid state, thermodynamic properties have been reliably predicted,[6,7] which show that molecular borane amine (BH_3NH_3), alane amine (AlH_3-NH_3), and alane phosphine (AlH_3PH_3) as well as the salts $[BH_4^-][NH_4^+]$, $[AlH_4^-][NH_4^+]$, $[AlH_4^-][PH_4^+]$, and $[BH_4^-][PH_4^+]$ can serve as hydrogen storage systems that release H_2. The ability to use borane amines for H_2 storage systems will also depend on the inherent H_2 release kinetics and mechanism of the processes.[4,5] Using thermoanalytical techniques, Wolf and co-workers[5] found that BH_3NH_3 begins to undergo stepwise thermal decomposition at a temperature as low as 410 K. During the first decomposition of solid borane amine, approximately 1 mol of H_2/mol BH_3NH_3 is released, together with formation of aminoborane, BH_2NH_2, and other polymeric derivatives. Elemental analysis and spectroscopic characterization by IR and X-ray diffraction methods, carried out by these authors,[5] clearly showed that thermal H_2 elimination (eq 1) requires moderate activation energy. In contrast, relatively little is known experimentally about the subsequent process (eq 2).[8]

$$BH_3NH_3 \rightarrow BH_2NH_2 + H_2 \quad (1)$$

$$BH_2NH_2 \rightarrow BHNH + H_2 \quad (2)$$

More recently, Li et al.[8] reported direct ab initio dynamics studies of reactions 1 and 2 with geometrical and energetic parameters obtained from different versions of the composite G3 and CBS methods. These authors identified a concerted mechanism with a planar four-member transition structure for H_2 elimination from BH_3NH_3, with an energy barrier of 32−33 kcal mol^{-1}. To reconcile this rather large energy barrier with the experimental kinetics mentioned above, they suggest that at low temperatures the rate constant is largely influenced by tunneling.[8a] Nevertheless, in their kinetic treatments, Li et al.[8a] did not include the B−N bond cleavage channel giving rise to BH_3 and NH_3. Evaluation of the $BH_3 + NH_3$ asymptote shows that it is 25.9 kcal mol^{-1} above the BH_3NH_3 molecule[6] and thus lies below the transition structure for H_2 elimination, so direct B−N dissociation is expected to be predominant over H_2 loss.

In this work, we report studies of the relevant H_2 release pathways in the BH_3NH_3 system, using high-level ab initio quantum chemical methods. We have tested the following hypothesis: during the transformation, can the BH_3 and/or NH_3 molecule(s) formed by bond cleavage of the B−N bond in BH_3-NH_3, act as a catalyst for H_2 production from the remaining BH_3NH_3 molecules? Our results show that the Lewis acid BH_3 molecule can effectively act as a bifunctional catalyst for the H_2 elimination. This type of reaction is related to hydrolysis reactions in aqueous solution where the solvent water molecules undergo an active solvent catalysis facilitating the water addition by a relay of H-transfers.[9] A number of catalysts have been developed recently to improve the rate of H_2 elimination from methyl-substituted boron amines.[10−13] To better understand the

* Corresponding author: e-mail dadixon@bama.ua.edu.
† The University of Alabama.
‡ University of Leuven.

10.1021/jp066175y CCC: $37.00
Published on Web 01/09/2007

catalytic reaction, we have also studied the electronic reorganization accompanying the H_2 release by using a topological analysis of the stationary points along the pathways. For a comparison and further extension of the scope of the catalytic mechanism, we have considered the H_2 elimination from the isoelectronic CH_3CH_3 without and with the presence of BH_3 as a catalyst.

Computational Methods

The calculations were performed by using the Gaussian-03[14] and MOLPRO-2006[15] suites of programs. The calculations were done on a variety of computers including the Cray XD-1 computer at the Alabama Supercomputer Center, a PQS Opteron computer at The University of Alabama, and the large HP Linux cluster in the Molecular Science Computing Facility at the William R. Wiley Environmental Molecular Sciences Laboratory at the Pacific Northwest National Laboratory. The geometries were initially optimized by use of density functional theory with the hybrid B3LYP exchange-correlation functional[16] in conjunction with the 6-311++G(d,p) basis set. The character of each stationary point was shown to be an equilibrium structure or a first-order saddle point by calculating the harmonic vibrational frequencies at the same level. To ascertain the identity of the relevant transition structures (TS), intrinsic reaction coordinate (IRC)[17] calculations were also done at the B3LYP/6-311++G-(d,p) level. Geometrical parameters were then reoptimized by use of the B3LYP functional and second-order perturbation theory (MP2)[18] and coupled-cluster CCSD(T) theory,[19] with the correlation-consistent aug-cc-pVTZ basis set.[20] The CCSD(T) optimizations were performed only for the BH_3NH_3 system.

For all of the molecular systems considered, single-point CCSD(T) electronic energies were performed with the aug-cc-pV*n*Z basis sets, with n = D, T, and Q (denoted hereafter as aV*n*Z), to extrapolate the CCSD(T) energies to the complete basis set (CBS) limit by use of the following expression:[21]

$$E(x) = A_{CBS} + B\exp[-(n-1)] + C\exp[-(n-1)^2] \quad (3)$$

with n = 2, 3, and 4 for the aug-cc-pV*n*Z, n = D, T, and Q basis sets, respectively. The single-point electronic energies for the atoms were calculated from the restricted coupled-cluster R/UCCSD(T) formalism. In this approach, a restricted open-shell Hartree−Fock (ROHF) calculation was initially performed and the spin constraint was relaxed in the coupled cluster calculation.[22−24]

For the systems for which CCSD(T)/aVTZ optimized geometries were not available, single-point CCSD(T) electronic energies were computed on the basis of the MP2/aVTZ-optimized geometries. In the MP2 and CCSD(T) calculations, the core orbitals were kept frozen. Harmonic vibrational frequencies computed at the MP2/aVTZ level were scaled to estimate the zero-point energies (ZPE) by use of scaling factors previously generated.[6]

Additional smaller energetic corrections including core-valence and relativistic corrections were also calculated following our previous work on calculating heats of formation based on total atomization energies (ΣD_0).[6,7] Core-valence corrections (ΔE_{CV}) were obtained at the CCSD(T)/cc-pwCVTZ level of theory.[25] Scalar relativistic corrections (ΔE_{SR}), which account for changes in the relativistic contributions to the total energies of the molecule and the constituent atoms, were included at the CISD (configuration interaction singles and doubles) level of theory by use of the cc-pVTZ basis set. ΔE_{SR} is taken as the sum of the mass−velocity and 1-electron Darwin (MVD) terms in the Breit−Pauli Hamiltonian.[26] Most calculations by available electronic structure computer codes do not correctly describe the lowest energy spin multiplet of an atomic state, as spin-orbit in the atom is usually not included. Instead, the energy is a weighted average of the available multiplets. The spin-orbit corrections are 0.08 kcal/mol for *C* and 0.03 kcal/mol for *B*, both from the excitation energies of Moore.[27]

In an attempt to better understand the electronic changes that occur on H_2 elimination, we used the atoms-in-molecules (AIM) approach.[28] The critical points (CPs) occur where the gradient of the electron density vanishes and allow us to define the atoms and chemical bonds within a molecule. In addition, an electron localization function (ELF) analysis was performed on the located minima and relevant transition structures.[29] Unless otherwise stated, bond distances are given in angstroms, bond angles in degrees, and relative energies in kilocalories per mole. Charges were calculated on the basis of natural bond orbitals (NBOs).[30]

Results and Discussion

Table 1 lists the different components of the calculated total atomization energies ΣD_0. Unless otherwise noted, the relative energies between stationary points quoted hereafter refer to the values obtained from the CCSD(T)/CBS-based total atomization energies. Cartesian coordinates of the stationary points optimized at the MP2/aVTZ level are given as Supporting Information (Table S1), as are the total electronic energies (Table S2) and the zero-point energies (ZPE), thermal corrections to enthalpies (TC), and entropies (*S*) (Table S3). For molecular hydrogen, ethane, ethylene, methyl radical, ammonia, and borane, the experimental ΣD_0 values[31] are also listed in Table 1. Table 2 gives a comparison of the energy barriers and reaction energies calculated at the different levels of theory.

Reaction Pathways for H_2 Release from Ethane. We first studied the Woodward−Hoffmann forbidden [2 + 2] loss of H_2 from C_2H_6. Selected geometrical parameters of the relevant transition structures, optimized by both the B3LYP and MP2 methods with the aVTZ basis set, are displayed in Figure 1. Relative energies between stationary points are schematically illustrated in Figure 2. We use the following labels: **TS** indicates a transition structure, **et** stands for ethane, and **b** represents an additional borane molecule. Figure 1 includes both **TSet** and **TSet-b** for H_2 release from ethane, without and with the presence of BH_3, respectively.

Table 1 shows that the relative energies calculated at the CCSD(T)/CBS level are in good agreement, within ±0.5 kcal/mol, with those derived from the well-established experimental heats of formation at 0 K for C_2H_6, C_2H_4, and CH_3. The energy of **TSet** rapidly converges to the CBS value (Table 2). The B3LYP and MP2 values differ by up to ±3 kcal/mol as compared to the CCSD(T)/CBS results. The results obtained at the CCSD(T)/aVTZ level are within ±1 kcal/mol with respect to the CBS limit.

TSet has C_s symmetry (Figure 1) and the H_2CCH_2 group that is being formed has a slightly *trans*-bent configuration. The departing H_2 molecule occupies a highly nonsymmetrical position. Both H-atoms are displaced in a parallel manner to the C−C bond, in such a way that both departing H atoms are centered at one carbon atom. This motion is well described by the normal mode of the corresponding imaginary frequency (see Figure S1 of Supporting Information). With a H−H bond distance of 1.15−1.20 Å as compared to a calculated bond distance of 0.74 Å in H_2, the H_2 is only weakly formed in **TSet**. There is a shorter C−H bond, only slightly extended by 0.1 Å

TABLE 1: Components for the Calculated Atomization Energies of Ethane and Related Structures[a]

molecule	CBS[b]	ΔE_{ZPE}[c]	ΔE_{CV}[d]	ΔE_{SR}[e]	ΔE_{SO}[f]	ΣD_0(0 K)	exptl. ΣD_0(0 K)[g]
CH_3CH_3	710.59	−46.40	2.18	−0.38	−0.17	665.82	666.3 ± 0.1
CH_3CH_3 **TS-et**	587.88	−39.72	1.97	−0.35	−0.17	549.33	
CH_2CH_2	561.75	−31.38	2.10	−0.32	−0.17	531.98	531.9 ± 0.1
H_2	109.44	−6.21	0.00	0.00	0.00	103.23	103.26 ± 0.1
CH_3	306.79	−18.40	0.96	−0.16	−0.08	289.11	289.3 ± 0.2
BH_3[h]	280.19	−16.20	0.98	−0.06	−0.03	264.88	264.6 ± 2.4
$CH_3CH_3 + BH_3$ **TSet-b**	924.91	−59.62	3.22	−0.41	−0.20	867.90	
BH_3NH_3[h]	609.26	−42.92	1.89	−0.39	−0.03	567.81	
BH_3NH_3 **TSba**[h]	569.02	−39.07	1.91	−0.40	−0.03	531.43	
BH_2NH_2[h]	499.63	−29.69	1.87	−0.38	−0.02	471.41	
NH_3[c]	297.43	−20.86	0.57	−0.26	0.0	276.88	276.7 ± 0.1
$BH_3NH_3 + BH_3$ **ba-com1**	910.66	−62.76	3.18	−0.46	−0.06	850.56	
$BH_3NH_3 + BH_3$ **TSba-BN**	883.46	−59.28	3.05	−0.46	−0.06	826.71	
$BH_3NH_3 + BH_3$ **TSba-BB**	838.39	−56.34	2.96	−0.43	−0.06	784.52	
$BH_3NH_3 + BH_3$ **TSba-lew**	861.24	−59.62	3.00	−0.44	−0.06	804.12	
BH_2NH_2-BH_3 **ba-ring**	814.74	−51.72	3.33	−0.48	−0.06	765.81	
$BH_3NH_3 + NH_3$ **ba-com2**	916.28	−65.86	2.55	−0.65	−0.03	852.29	
$BH_3NH_3 + NH_3$ **TSba-NB**	881.70	−62.42	2.51	−0.66	−0.03	821.10	
$BH_3NH_3 + NH_3$ **TSba-NN**	803.71	−58.73	2.62	−0.67	−0.03	746.90	
$BH_3NH_3 + NH_3$ **TSba-NH$_3$**	871.41	−61.45	2.53	−0.67	−0.03	811.79	

[a] Energies are given in kilocalories per mole. [b] From CCSD(T)/CBS energies extrapolated by use of eq 3, with aV*n*Z basis sets, where n = D, T, and Q, based on MP2/aVTZ optimized geometries, unless otherwise noted. Total energies are given in Table S2 (Supporting Information). [c] Calculated zero-point energies (see Table S2). A scaling factor of 0.97 obtained from ethane, ethylene, borane, and ammonia was applied for the transition structures. The other values were taken from refs 6 and 7. [d] Core/valence corrections were obtained at the CCSD(T/cc-pwCVTZ basis set level. [e] Scalar relativistic corrections (MVD) from CISD/aVTZ calculations. [f] Atomic spin-orbit correction. [g] Experimental values are taken from ref 31. [h] Based on CCSD(T)/aVTZ optimized geometries.

TABLE 2: Energy Barriers ($\Delta H^{\ddagger}$) and Reaction Energies (ΔH_R) of the H_2 Release Reactions from Ethane and Borane Amine at Different Levels of Theory[a]

parameter	MP2/aVTZ	CCSD(T)/aVDZ	CCSD(T)/aVTZ	CCSD(T)/aVQZ	CCSD(T)/CBS
		$CH_3CH_3 \rightarrow CH_2CH_2 + H_2$			
$\Delta H^{\ddagger}$ **TSet**	117.4	115.6	116.4	116.4	116.4
ΔH_R	32.7	31.5	31.3	31.0	30.8
		$CH_3CH_3 \rightarrow 2CH_3$			
ΔH_R	90.4	86.1	86.6	87.3	87.8
		$CH_3CH_3 + BH_3 \rightarrow CH_2CH_2 + H_2 + BH_3$			
$\Delta H^{\ddagger}$ **TSet-b**	62.6	62.6	63.3	63.2	63.2
		$BH_3NH_3 \rightarrow BH_2NH_2 + H_2$			
$\Delta H^{\ddagger}$ **TSba**	35.5	37.4	36.8	36.5	36.4
ΔH_R	−6.8	−5.6	−6.4	−6.8	−7.0
		$BH_3NH_3 + BH_3 \rightarrow BH_2NH_2 + H_2 + BH_3$			
ΔH_R complex	−18.3	−16.5	−17.6	−17.7	−17.7
$\Delta H^{\ddagger}$ **TSba-BN**	5.0	7.6	6.4	6.1	6.0
$\Delta H^{\ddagger}$ **TSba-BB**	47.0	47.9	48.1	48.1	48.1
$\Delta H^{\ddagger}$ **TSba-lew**	26.4	30.1	28.5	28.5	28.5
		$BH_3NH_3 + NH_3 \rightarrow BH_2NH_2 + H_2 + NH_3$			
ΔH_R complex	−8.2	−9.1	−8.0	−7.9	−7.8
$\Delta H^{\ddagger}$ **TSba-NB**	22.2	23.4	23.5	23.4	23.4
$\Delta H^{\ddagger}$ **TSba-NN**	96.5	96.6	97.5	97.6	97.7
$\Delta H^{\ddagger}$ **TSba-NH$_3$**	31.6	33.4	32.9	32.8	32.7

[a] Energies, in kilocalories per mole, are based on total energies listed in Table S2 and zero-point energies given in Table S3 if not taken from Table 1.

from a normal C−H bond, and this corresponds to the H transferred from one CH_3 to the other. The other C−H bond is much longer, near 1.5 Å. The C−C bond of 1.44−1.45 Å falls between those of single (1.524 Å) and double (1.333 Å) carbon−carbon bonds calculated at the MP2/aVTZ level.

TSet corresponds to a structure with the H from one CH_3 group partially dissociated and with the H from the other CH_3 group partially attached to the CH_3 group that is losing a hydrogen and is, in fact, almost fully transferred to the other CH_3 group. Figure 2 clearly shows that the unimolecular H_2 elimination from ethane via **TSet** is characterized by an extremely high-energy barrier of about 117 kcal/mol, consistent with a Woodward−Hoffmann forbidden reaction. Such a barrier height is substantially larger than any of the bond dissociation energies (BDEs) of ethane, BDE(C−C) = 87.7 kcal/mol and BDE(C−H) = 100.8 kcal/mol,[22] just as found for the $H_2 + H_2$ four-center exchange reaction.[32] In **TSet,** the migrating H_2 moiety is positively charged, in which the outermost H-atom bears a small negative charge of −0.07 electron, and the other has a positive charge of 0.36 electron. The charge distribution in **TSet** resembles more a $H\bullet/C_2H_5\bullet$ pair or $H_2^+/C_2H_4^-$ rather than an $H^-/C_2H_5^+$ pair. The forming H−H has a bond order of only 0.13, consistent with the long H−H bond distance. The two C−H bonds connecting the carbon with these H atoms have bond orders of 0.57 and 0.36, consistent with the bond distances given in Figure 1.

We now consider H_2 elimination from ethane in the presence of the Lewis acid borane. There is an initial weak complex

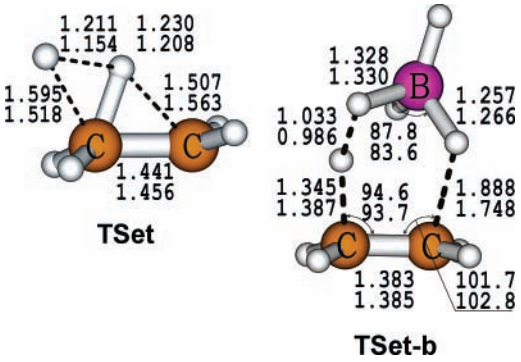

Figure 1. Geometrical parameters of transition state structures for H_2 release from ethane without, **TSet**, and with the presence of borane, **TSet-b**. (Upper) B3LYP/aVTZ; (lower) MP2/aVTZ.

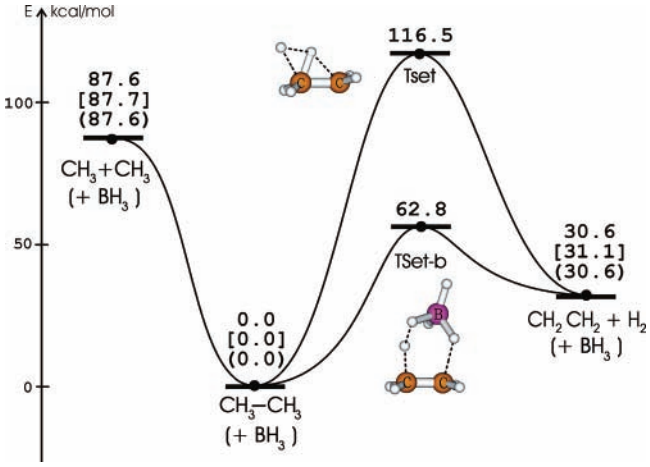

Figure 2. Schematic energy profiles showing the reaction pathways for H_2 release from ethane without (via **TSet**) and with (via **TSet-b**) the presence of BH_3. Entries for relative energies (kilocalories per mole) are, for ethane, CCSD(T)/CBS values followed by experimental results in brackets; for ethane + BH_3, CCSD(T)/CBS results are given in parentheses.

involving CH_3CH_3 and BH_3, with a binding energy of less than −0.5 kcal/mol (not shown on the diagram). From the separated reactants, the pathway passes through **TSet-b** shown in Figure 1. In this six-membered cyclic transition state structure, a H from ethane is transferred to a H on the borane. The other H from ethane is already transferred to the Lewis acidic borane. The C−C distance is substantially compressed, comparable to that of a typical double bond (1.33 Å), whereas the B−H bond accepting the H that will eventually form the H_2 is 1.33 Å, somewhat longer than a B−H bond of 1.20 Å. The other H atom transferred from C_2H_6 has made a strong B−H bond which is elongated by <0.1 Å as compared to a normal B−H bond. The H−H distance of about 1.0 Å points out the H_2 existence. The IRC calculations show that the initial products from **TSet-b** are BH_5 + C_2H_4. BH_5 is best described as a weak complex between H_2 and BH_3,[33] and it is clear from the normal mode of the imaginary frequency (Figure S1 in Supporting Information) that two H-atoms of ethane are captured by BH_3 as H_2. The geometry of BH_5 at the MP2/aVTZ level has a short H−H bond of 0.799 Å and B−H bonds of 1.405 and 1.421 Å. The H_2 entity has a positive charge of 0.18 e resulting from a net electron transfer from BH_3.

The calculated electron populations of **TSet-b** are shown in Figure S2, together with the bond critical points. The bond orders show substantial bond formation and breakage in the transition state structure. Electron transfer from ethane to borane is relatively small (−0.1 e) in **TSet-b**. The net charges within

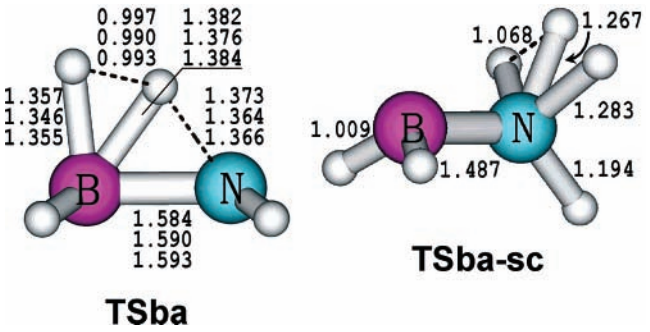

Figure 3. Geometrical parameters of transition state structure **TSba** optimized by use of, in order, B3LYP/aVTZ, MP2/aVTZ, and CCSD-(T)/aVTZ. Geometry of **TSba-sc** optimized at the MP2/aVTZ level. Structure **TSba** has a plane of symmetry (that of the page) so there is a symmetry equivalent H on both B and N that is behind the page and not shown.

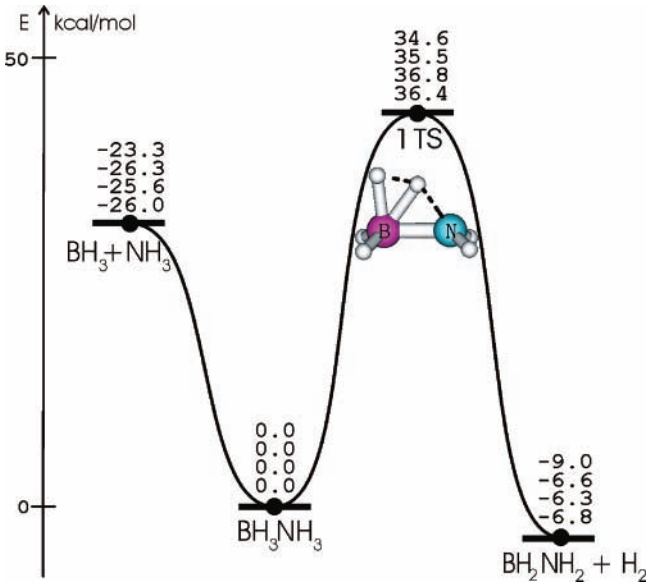

Figure 4. Reaction pathways from BH_3NH_3. Relative energies in kilocalories per mole are given in order from top to bottom: B3LYP/aVTZ, MP2/aVTZ, CCSD(T)/aVTZ, and CSD(T)/CBS, respectively. ZPEs were derived from B3LYP for the first entry and from MP2 for the others.

the ($C^{\delta-}$-$H^{\delta+}$-$H^{\delta-}$-$B^{\delta-}$) framework for **TSet-b** show a partially formed dihydrogen bond, which is additionally stabilized by electrostatic interactions.[34] Thus, the electron redistribution in **TSet-b** shows that borane is a bifunctional catalyst, which has both acidic (H-atom donation) and basic (H-atom acceptance) character, in the Brønsted−Lowry definition. The energetic consequence of the addition of BH_3 is to lower substantially the energy barrier via **TSet-b** to 62.8 kcal/mol, a reduction of 53.7 kcal/mol, relative to the unimolecular loss of H_2 from ethane.

Reaction Pathways for H_2 Release from BH_3NH_3. The calculated results for the unimolecular decomposition of borane amine are summarized in Figures 3 and 4. Parameters for the equilibrium structures BH_3NH_3 and BH_2NH_2 have been reported and analyzed in detail.[6] Table 2 shows that the CCSD(T)/aVTZ relative energies are found to differ from CCSD(T)/CBS counterparts by only up to 0.4 kcal/mol. There are only minor differences between the MP2 and CCSD(T) sets of geometries, and as a consequence, the use of MP2-optimized geometries for the CCSD(T) energies leads to only small variations in the energies, on the order of 0.2 kcal/mol. Overall, relative energies

determined from single-point CCSD(T)/aVTZ//MP2/aVTZ energies deviate by, at most, ±1.0 kcal/mol from the CBS limit values.

The shape and geometrical parameters for **TSba** (**ba** stands for borane amine) are shown in Figure 3. The results reported in ref 8a for the B3LYP functional with smaller basis sets are comparable to those given in Figure 3. As in the ethane case, loss of H_2 is highly asymmetrical and the transition state structure geometries for loss of H_2 from BH_3NH_3 are similar to those for loss of H_2 from C_2H_6. The NH_3 group transfers a hydrogen to the boron center and the B−H bond elongates so that the two long B−H distances are now comparable. The H−H distance of around 1.0 Å is substantially shorter than that of 1.2 Å in **TSet**, so there is more H−H bond formation in **TSba**.

A second transition state structure, denoted as **TSba-sc**, was also located and its MP2/aVTZ geometries are also given in Figure 3. This transition state structure contains four H-atoms around the N-atom. The short central H−H distance of 1.07 Å is longer than that of **TSba**. However, IRC calculations reveal that **TSba-sc** is a transition state structure for hydrogen scrambling, yielding in both directions $BH_2NH_2 + H_2$ fragments, and does not lead back to BH_3NH_3. A similar transition state structure also exists in the parent BH_5 system,[33] and therefore, this transition state structure was not further considered.

Our best calculations predict that **TSba** is 36.4 kcal/mol above the BH_3NH_3 molecule and 10.4 kcal/mol above the $BH_3 + NH_3$ asymptote (Figure 4). Such energy barriers are markedly smaller than those found above for the isoelectronic ethane via **TSet** (Figure 2). The major differences between C_2H_6 and BH_3NH_3 are the high polarity and weak nature of the B−N dative σ bond relative to the nonpolar C−C σ bond. In addition, the strength of the forming σ bond in BH_2NH_2 is likely to be important.[6]

We performed a kinetic analysis, considering both the B−N bond dissociation and H_2 loss channels and using the RRKM theory for unimolecular reactions[35] with the rate expression

$$k_{\text{uni}} = \frac{\sigma}{h}\left[\frac{(N^{\ddagger})E - E_0}{\rho(E)}\right] \tag{4}$$

where σ is the symmetry number. Evaluation of the sum ($N^{\ddagger}$) and density (ρ) of states was carried out with the KHIMERA program.[36] The rate constant as a function of temperature (T) and pressure of the bath gas (p) for the range of T from 200 to 2000 K and p from 0.1 to 8360 Torr is given in Figure 5. We used the MP2/aVTZ geometries and vibrational frequencies combined with CCSD(T)/CBS total electronic energies. For this range of T and p with N_2 as the collision gas, the calculated rate constants can be fit to the following general expressions (energy in kilocalories per mole):

$$k(T,p)_{\text{H}_2} = (1.00 \times 10^{11})p^{0.55} \exp\frac{-35.6}{RT} \tag{5}$$

$$k(T,p)_{\text{B-N}} = (2.65 \times 10^{9})p^{0.96} \exp\frac{-21.9}{RT} \tag{6}$$

At 298 K and 760 Torr, $k_{\text{H}_2} = 4.6 \times 10^{-14}$ s^{-1} and $k_{\text{B-N}} = 2.7 \times 10^{-4}$ s^{-1}; at 373 K and 760 Torr, $k_{\text{H}_2} = 1.2 \times 10^{-8}$ s^{-1} and $k_{\text{B-N}} = 1.4$ s^{-1}. We treated the B−N dative bond-breaking reaction as a reaction with no barrier other than the endothermicity for breaking the bond (see Supporting Information Figure S2 for a plot of this process obtained at the B3LYP/DGDZVP2 level). At a high pressure of 8360 Torr (11 atm), the decomposition thermal rate coefficients are $k_{\text{H}_2} = 4.6 \times 10^{-14}$ s^{-1} and $k_{\text{B-N}} = 1.3 \times 10^{-3}$ s^{-1} at 298 K. For H_2 elimination, the rate

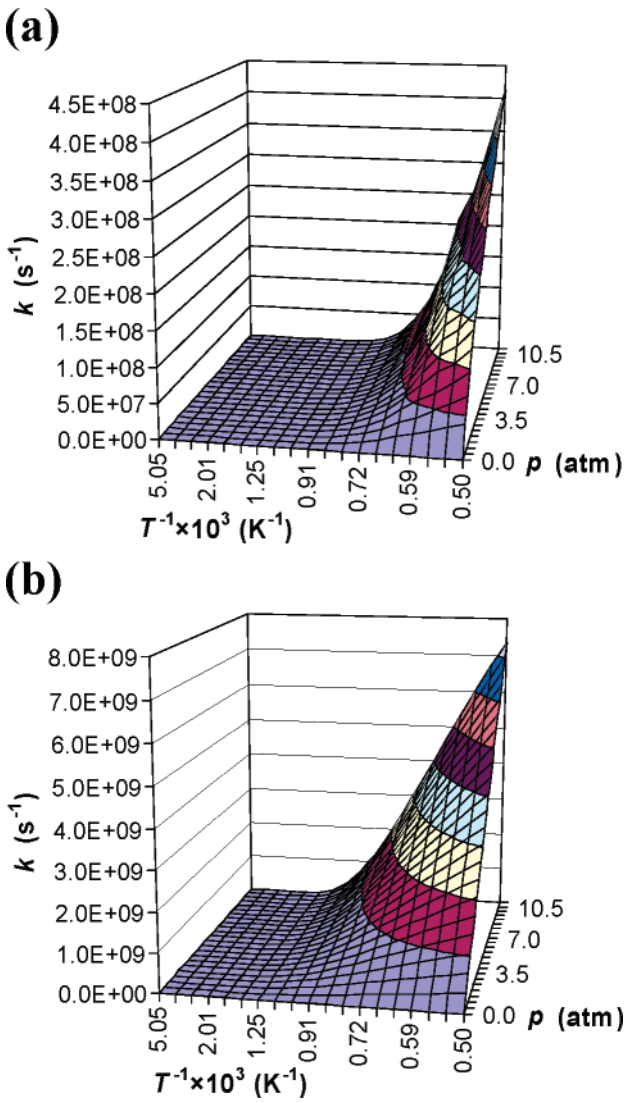

Figure 5. Three-dimensional plots of the rate coefficients $k(T, p)$ for (a) H_2 release, and (b) B−N bond cleavage in borane amine, using the RRKM method with N_2 as the bath gas in the temperature range (T) from 200 to 2000 K and pressure range (p) from 0.1 to 8360 Torr.

constants at 1 and 11 atm are the same so that the high-pressure limit has been reached at 1 atm.

The high-pressure thermal rate constant, in the thermodynamic formulation (TST, transition-state theory),[37,38] is given by

$$k_{\infty}(\text{TST}) = \frac{k_{\text{B}}T}{h}\exp\frac{\Delta S^{\ddagger}}{R}\exp\frac{-\Delta H^{\ddagger}}{RT} \tag{7}$$

and the high-pressure limit pre-exponential factor is thus given by $A = (k_{\text{B}}T/h)\exp(\Delta S^{\ddagger}/R)$. E_a of the Arrhenius expression[35,37] from TST and $\Delta H^{\ddagger}$ are related by $E_a = \Delta H^{\ddagger} + RT$ for a unimolecular process, so in our case $E_a = 37.0$ kcal/mol. For the hydrogen elimination, $k_{\infty,\text{H}_2}(\text{TST}) = 3.7 \times 10^{-14}$ s^{-1} at 298 K and 1.0×10^{-8} s^{-1} at 373 K; these values are very similar to those calculated by use of RRKM theory at high pressure.

In the above treatment, we have not included any correction for quantum mechanical tunneling. Due to the presence of a barrier of finite height and width (transition-state frequency of 1467i cm^{-1} for H_2 elimination) between the reactants and the dissociated products, there will be a tunneling correction to the rate constant. The simplest estimate of the tunneling effect $Q_{\text{tunnel,W}}$, comes from the Wigner[39] expression:

$$Q_{\text{tunnel,W}}(T) = 1 + \frac{1}{24}\left(\frac{h\omega_i}{k_B T}\right)^2 \quad (8)$$

At 298 K, $Q_{\text{tunnel,W}} = 1.88$, and at 373 K, it is 1.54 for the H_2 elimination reaction via **TSba**. Applying this correction, we obtain $k_{H_2}(298\text{ K}) = 8.6 \times 10^{-14}\ s^{-1}$ and $k_{H_2}(373\text{ K}) = 1.9 \times 10^{-8}\ s^{-1}$, for the RRKM method, both at 1 atm and at high pressure (11 atm). These RRKM high-pressure values are similar to those obtained by the TST method, $k_{\infty,H_2}(\text{TST}) = 7.0 \times 10^{-14}\ s^{-1}$ at 298 K and $1.6 \times 10^{-8}\ s^{-1}$ at 373 K. The $Q_{\text{tunnel,W}}$ values as a function of temperatures are listed in Table S4.

Skodje and Truhlar[40] derived an improved tunneling approximation which includes not only the imaginary frequency but also the energy barrier and the reaction energy, as given in eq 9, where $\Delta H^{\ddagger}$ is the zero-point-corrected barrier height and ΔH_R is the reaction exothermicity, both at 0 K:

$$Q_{\text{tunnel,ST}}(T) = \frac{\beta\pi/\alpha}{\sin(\beta\pi/\alpha)} - \frac{\beta}{\alpha - \beta}\exp[(\beta - \alpha)(\Delta H^{\ddagger} - \Delta H_R)] \quad \text{for } \alpha \geq \beta \quad (9a)$$

$$Q_{\text{tunnel,ST}}(T) = \frac{\beta}{\beta - \alpha}\{\exp[(\beta - \alpha)(\Delta H^{\ddagger} - \Delta H_R)] - 1\} \quad \text{for } \beta \geq \alpha \quad (9b)$$

with $\beta = 1/k_B T$ and $\alpha = 2\pi/h\omega_i$, where ω_i is the imaginary frequency at the transition state; when the reaction is exoergic, ΔH_R is equal to zero. At 298 K, $Q_{\text{tunnel,ST}} = 9.0 \times 10^3$, and at 373 K, it is 9.11, for the H_2 elimination (with **TSba**). These tunneling factors are much larger than those calculated by the Wigner equation and should be more reliable. Large tunneling corrections have been previously found. For example, Zuev et al.[41] found that, for halogenated carbene reactions at very low temperatures, the tunneling contributions to the rate constant can be up to 152 orders of magnitude greater than the rate constant without tunneling. By applying the corresponding correction to the RRKM values, we obtain $k_{H_2}(298\text{ K}) = 4.1 \times 10^{-10}\ s^{-1}$ and $k_{H_2}(373\text{ K}) = 1.1 \times 10^{-7}\ s^{-1}$, at both 1 and 11 atm. These values are very similar to those obtained by TST: $k_{\infty,H_2}(\text{TST, 298 K}) = 6.3 \times 10^{-10}\ s^{-1}$ and $k_{\infty,H_2}(\text{TST, 373 K}) = 9.1 \times 10^{-8}\ s^{-1}$.

Table 3 shows the values of the rate constants obtained by RRKM and TST with and without the tunneling. In addition, Figure 5 shows, in the temperature and pressure regimes of interest, that B−N bond cleavage is completely dominant over H_2 release, consistent with the energy profile shown in Figure 4.

Reaction Pathway for H_2 Release from BH_3NH_3 in the Presence of BH_3. Having confirmed the unfavorable pathway for H_2 loss from the borane amine monomer, we now consider the H_2 release mechanism involving an additional borane molecule. Geometrical parameters of the relevant stationary points, optimized at both B3LYP and MP2 levels with the aVTZ basis set, are shown in Figure 6. Normal modes for the imaginary frequencies of **TSba** and **TSba-BN** are shown in Figure S3. Single-point electronic energies were computed at the CCSD(T)/aV*n*Z//MP2/aVTZ level. To facilitate the comparison, relative energies along the reaction pathways obtained by four selected levels of theory are summarized in Figure 7. Although the energy ordering remains unchanged, the variation among the relative values obtained by the B3LYP method is up to 4 kcal/mol with respect to the CBS values. With the aVTZ basis set, the MP2 and CCSD(T) results differ by ±2.0 kcal/mol from each other, and the CCSD(T)/aVTZ results differ by ±0.5 kcal/mol from the CBS limit. Unless otherwise stated, the values quoted hereafter refer to the CCSD(T)/CBS results.

A strong complex between BH_3NH_3 and BH_3 is initially formed (**ba-com1** in Figure 6) and is 17.9 kcal/mol more stable than the $BH_3NH_3 + BH_3$ asymptote (Figure 7). Three transition state structures, rather than one as in the case of ethane, have been located and selected geometry parameters are also displayed in Figure 6. Each of these transition state structures represents a distinct type of interaction exerted by BH_3 on H_2 formation. **TSba-lew** corresponds to a process in which the BH_3 interacts with the **TSba** of the monomer. Parameters within the four-membered B−N−H−H rings in both transition state structures are comparable to each other. The B−N bond in the original BH_3-NH_3 substantially elongates by about 0.2 Å when the additional BH_3 is introduced to the complex. Because the N−H bond for the hydrogen being transferred is substantially broken in the transition state, the N and B from the original BH_3NH_3 start to form the B−N σ-bond needed in the product BH_2NH_2. Thus, the B from the original BH_3NH_3 begins to resemble a BH_2 complexed to an H_2 just as in **TSba**. This frees up part of the lone pair on the N and the incoming BH_3 molecule can interact with this partial lone pair, leading to an overall stabilization. Thus, the BH_3 plays the role of a classical Lewis acid interacting with the lone pair on N to stabilize the transition state structure framework for H_2 loss. Relative to the separated reactants, **TSba-lew** is calculated to be 28.6 kcal/mol higher in energy. Compared to decomposition of the BH_3NH_3 monomer, this corresponds to a decrease of 7.8 kcal/mol in the energy barrier. Starting from the complex **ba-com1**, the barrier height becomes 46.5 kcal/mol (Figure 7). It is of interest that the product of this process is the three-membered ring **ba-ring**, which results from a condensation of BH_2NH_2 and BH_3 and features a three-center B−H−B bond like that in diborane. Such a condensation is exothermic by −29.6 kcal/mol.

Both **TSba-BB** and **TSba-BN** are similar to **TSet-b** discussed above as the BH_3 plays an active role in the transition state structure for H_2 formation by giving and receiving H atoms. Both transition state structures feature some similarities but also many important differences. The letters **BB** and **BN** stand for the appearance of the B−H−H−B and B−H−H−N chains in these structures, respectively. In fact, this point constitutes the main difference between them. IRC calculations show that both transition state structures connect to the same reactants (the preassociation complex **ba-com1)** and the $BH_2NH_2 + H_2 + BH_3$ products.

The B−N distance is shorter than the bond distance of 1.65 Å in BH_3NH_3, about 1.49 Å in both structures, but remains longer than that of 1.41 Å in BH_2NH_2.[6] **TSba-BB** appears to be more distorted than **TSba-BN**, having a small H−B−H bond angle and more stretched B−H bonds. **TSba-BB** is essentially the same as found in **TSet-b** with an H transferred from N to the BH_3 and an H from the BH_3 in BH_3NH_3 transferred to an H on the BH_3 catalyst. In **TSba-BN,** the situation is reversed with the B transferring an H to the BH_3 catalyst and the N transferring an H to an H on the BH_3 catalyst. The transfer of two H atoms from BH_3NH_3 to BH_3 should be significantly faster in **TSba-BN** than in **TSba-BB**, in particular for the H(B) bond formation. In the former, with a distance of about 0.9 Å, the new H−H molecule is virtually formed, and along with shorter B−H distances, a BH_5 moiety appears to already exist. As in **TSet-ba**, although the latter looks more like a perturbed BH_4 group interacting with a BH_3NH_2, the calculated NBO populations indicate that there is no formal charge separation. The bond critical points, atomic charges, and bond order were

TABLE 3: Rate Constants of the Different Reactions[a]

	at 298 K			at 373 K		
method	no tunneling	W	ST	no tunneling	W	ST
			$BH_3NH_3 \rightarrow BH_3 + NH_3$			
RRKM at 1 atm	2.7×10^{-4}			1.4		
RRKM at 11 atm	1.3×10^{-3}			8.6		
			$BH_3NH_3 \rightarrow BH_2NH_2 + H_2$			
RRKM at 1 atm	4.6×10^{-14}	8.6×10^{-14}	4.1×10^{-10}	1.2×10^{-8}	1.9×10^{-8}	1.1×10^{-7}
RRKM at 11 atm	4.6×10^{-14}	8.6×10^{-14}	4.1×10^{-10}	1.2×10^{-8}	1.9×10^{-8}	1.1×10^{-7}
TST	3.7×10^{-14}	7.0×10^{-14}	6.3×10^{-10}	1.0×10^{-8}	1.6×10^{-8}	9.1×10^{-8}
			$BH_3NH_3 \cdots BH_3 \rightarrow BH_2NH_2 + H_2 + BH_3$			
RRKM at 1 atm	2.8×10^{-5}	4.1×10^{-5}	5.9×10^{-5}	8.1×10^{-2}	1.1×10^{-1}	1.3×10^{-1}
RRKM at 11 atm	2.8×10^{-5}	4.1×10^{-5}	5.9×10^{-5}	8.1×10^{-2}	1.1×10^{-1}	1.3×10^{-1}
TST	2.9×10^{-5}	4.3×10^{-5}	6.1×10^{-5}	8.5×10^{-2}	1.1×10^{-1}	1.3×10^{-1}
			$BH_3NH_3 + BH_3 \rightarrow BH_2NH_2 + H_2 + BH_3$			
TST (bimolecular)	3.6×10^{6}	5.3×10^{6}	7.5×10^{6}	2.5×10^{7}	3.3×10^{7}	3.9×10^{7}
			$BH_3NH_3 \cdots NH_3 \rightarrow BH_2NH_2 + H_2 + NH_3$			
RRKM at 1 atm	8.2×10^{-12}	1.3×10^{-11}	2.2×10^{-11}	2.8×10^{-7}	3.8×10^{-7}	5.0×10^{-7}
RRKM at 11 atm	8.2×10^{-12}	1.3×10^{-11}	2.2×10^{-11}	2.8×10^{-7}	3.8×10^{-7}	5.0×10^{-7}
TST	6.9×10^{-12}	1.1×10^{-11}	1.8×10^{-11}	2.5×10^{-7}	3.4×10^{-7}	6.0×10^{-7}
			$BH_3NH_3 + NH_3 \rightarrow BH_2NH_2 + H_2 + NH_3$			
TST (bimolecular)	6.7×10^{-7}	1.0×10^{-6}	1.8×10^{-6}	2.9×10^{-3}	3.9×10^{-3}	6.9×10^{-3}

[a] Rate constants were calculated at room temperature (298 K) and 373 K without and with tunneling corrections calculated by the Wigner (W) and Skodje and Truhlar (ST) approximations. Units are per second (for unimolecular reactions) and cubic centimeters per mole per second (for bimolecular reactions).

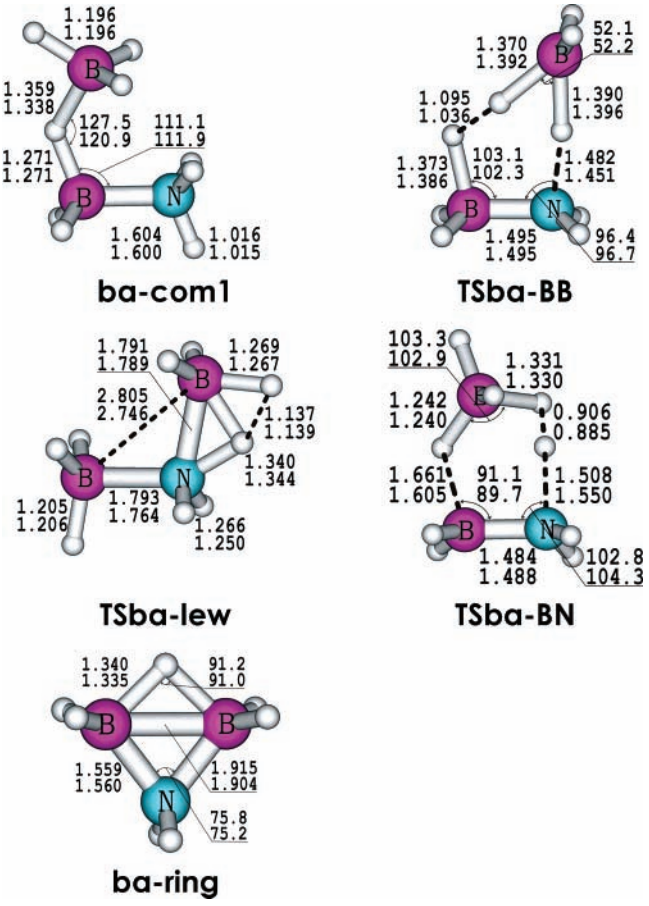

Figure 6. Geometrical parameters of the initial complex **ba-com1,** product **ba-ring**, and transition state structures **TSba-BN**, **TSba-lew**, and **TSba-BB** optimized with B3LYP/aVTZ (upper) and MP2/aVTZ (lower). Bond lengths are given in angstroms and bond angles in degrees.

calculated with B3LYP/6-311++G(d,p) and are shown in Figure 8 for both **TSba** and **TSba-BN**. H−H bond formation is more advanced in the catalyzed **TSba-BN** than in the monomer **TSba**.

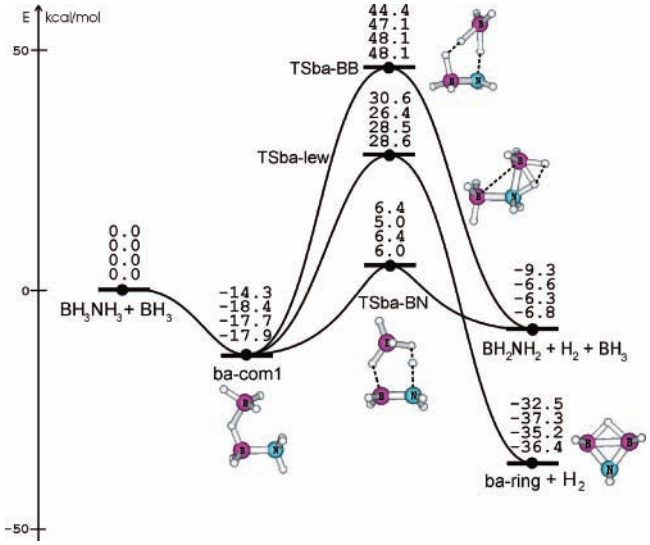

Figure 7. Schematic energy profiles illustrating H_2 release from BH_3-NH_3 with the presence of BH_3. Relative energies in kilocalories per mole are given in order from top to bottom: B3LYP/aVTZ, MP2/aVTZ, CCSD(T)/aVTZ, and CCSD(T)/CBS.

The bond order of the breaking B−H bond is about 0.5 in comparison with 0.7 for the forming B−H bond. In both cases, the B−N bond order is higher than 0.7. It is known that protonation of BH_2NH_2 takes place at the N-site, giving BH_2-NH_3^+ rather than $BH_3NH_2^+$.[42] **TSba-BN** is far more stable than **TSba-BB**, with an energy difference of 42.1 kcal/mol in favor of the former (Figure 7). This places **TSba-BN** at only 6.0 kcal/mol above the energy of separated reactants and 23.9 kcal/mol above **ba-com1**. Thus, only the process via **TSba-BN** proceeds with low energy.

To evaluate the rate coefficients of the catalytic process, we have considered two distinct channels. The first starts from the separated reactants and connects directly to **TSba-NB.** The rate constants of this bimolecular reaction can be evaluated by conventional transition-state theory (TST).[37,38] The calculated data can be fit to a three-parameter expression as $k(T) =$

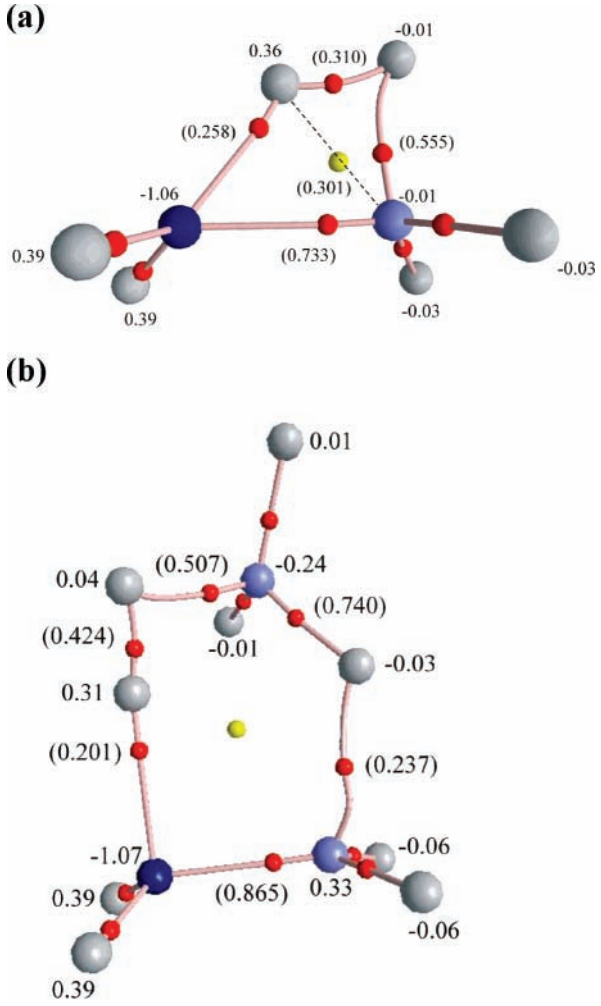

Figure 8. Molecular graphs of transition state structures (a) **TSba** and (b) **TSba-BN** (red, bond critical points; dark blue, carbon atoms; gray, hydrogen atoms; and violet, boron). NBO charges were from B3LYP/6-311++G(d,p) calculations. Bond orders are shown in parentheses.

$(1.5 \times 10^2)T^{2.89}$ exp($-3.88/RT$) cm^3 molecule^{-1} s^{-1} for the temperature range T from 200 to 2000 K. The simple Arrhenius expression

$$k = A \exp\left(\frac{-E_a}{RT}\right) \tag{10}$$

gives $k(T) = (5.0 \times 10^{11})$ exp($-6.96/RT$) cm^3 molecule^{-1} s^{-1}. At 298 K, the rate constant is $k = 3.6 \times 10^6$ cm^3 molecule^{-1} s^{-1}, and at 373 K, it is $k = 2.5 \times 10^7$ cm^3 molecule^{-1} s^{-1}.

If the association complex **ba-com1** in the entrance channel is stabilized by collisions, the rate constant will be different than if the complex is not stabilized. We can then use both TST and RRKM theory to predict the rate for unimolecular decomposition of **ba-com1**, via **TSba-BN.** By use of eq 7, the TST rate coefficients (high-pressure limit) are calculated as $k(T) = (2.5 \times 10^{10})T^{0.78}$ exp($-23.0/RT$) s^{-1}. At room temperature the high-pressure rate coefficient is k_∞(298 K) $= 2.9 \times 10^{-5}$ s^{-1}, and at 373 K it is k_∞(373 K) $= 8.5 \times 10^{-2}$ s^{-1}. We also employed eq 4 to evaluate the temperature and pressure dependence of the rate constants. Figure 9 displays a 3D graphic representing the variations of $k(T, p)$, with the same ranges of T and p given above with N_2 as the collision gas, which yields

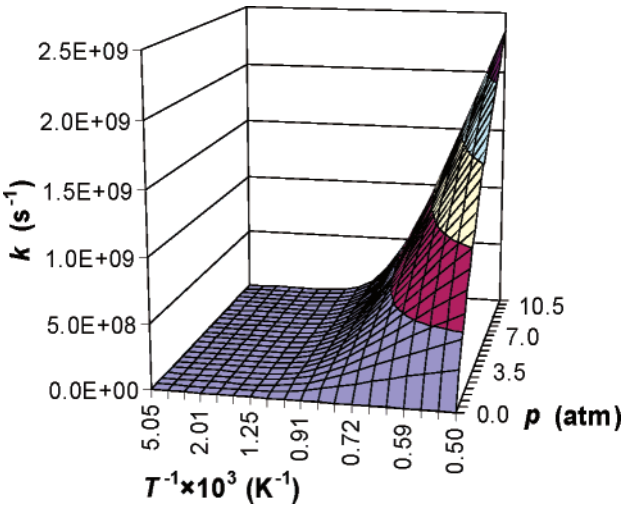

Figure 9. Three-dimensional plot of the rate coefficients $k(T, p)$ of H_2 release from borane amine with BH_3 as a catalyst via **TSba-BN**, using the RRKM method with N_2 as the bath gas in the temperature range (T) from 200 to 2000 K and pressure range (p) from 0.1 to 8360 Torr.

the following expression for the rate constant as a function of T and p:

$$k(T,p) = (2.0 \times 10^{10})p^{0.52} \exp\frac{-22.4}{RT} \tag{11}$$

The high-pressure RRKM rate constants for the unimolecular rearrangement **ba-com1** → **TSba-BN** are k_∞(298 K) $= 2.8 \times 10^{-5}$ s^{-1} and k_∞(373 K) $= 8.1 \times 10^{-2}$ s^{-1}, essentially those obtained by the TST approximation. These values are also the same as those at 1 atm, which means that the reaction has reached the pressure limit at 1 atm.

To evaluate the tunneling correction, we used both the Wigner and the Skodje and Truhlar expressions. The calculated imaginary frequency for **TSba-BN** is $\omega_i = 805i$ cm^{-1} at the MP2/aVTZ level. From this value, we obtain a value for $Q_{tunnel,W}$(298 K) $= 1.48$ and $Q_{tunnel,W}$(373 K) $= 1.31$ from eq 8 for both bimolecular and unimolecular processes.

At room temperature and at 373 K, the tunneling corrected RRKM rate constants are k(298 K) $= 4.1 \times 10^{-5}$ s^{-1} and k(373 K) $= 1.1 \times 10^{-1}$ s^{-1} at both 1 and 11 atm. Very similar results are found when the corresponding corrections are applied to the TST results: k_∞(TST, 298 K)$= 4.3 \times 10^{-5}$ s^{-1} and k_∞(TST, 373 K)$= 1.1 \times 10^{-1}$ s^{-1}. For the bimolecular reaction we have k(298 K) $= 5.3 \times 10^6$ cm^3 molecule^{-1} s^{-1} and k(373 K) $= 3.3 \times 10^7$ cm^3 molecule^{-1} s^{-1}.

In comparison we obtain $Q_{tunnel,ST}$(298 K) $= 2.09$ and $Q_{tunnel,ST}$(373 K) $= 1.55$, and in this case, the unimolecular and bimolecular reactions produce the same tunneling factor from eq 9. At room temperature and at 373 K, the tunneling-corrected RRKM rate constants are k(298 K) $= 5.9 \times 10^{-5}$ s^{-1} and k(373 K) $= 1.3 \times 10^{-1}$ s^{-1}, for both 1 and 11 atm, and again, very similar values are found for the TST results: k_∞(TST, 298 K) $= 6.1 \times 10^{-5}$ s^{-1} and k_∞(TST, 373 K) $= 1.3 \times 10^{-1}$ s^{-1}. For the bimolecular reaction we have k(298 K) $= 7.5 \times 10^6$ cm^3 molecule^{-1} s^{-1} and k(373 K) $= 3.9 \times 10^7$ cm^3 molecule^{-1} s^{-1}. The Q_{tunnel} values as a function of temperatures are listed in Table S4, and the different values for the rate coefficients are shown in Table 3.

Reaction Pathway for H_2 Release from BH_3NH_3 in the Presence of NH_3. We also studied whether an ammonia molecule (produced by bond cleavage of borane amine) could

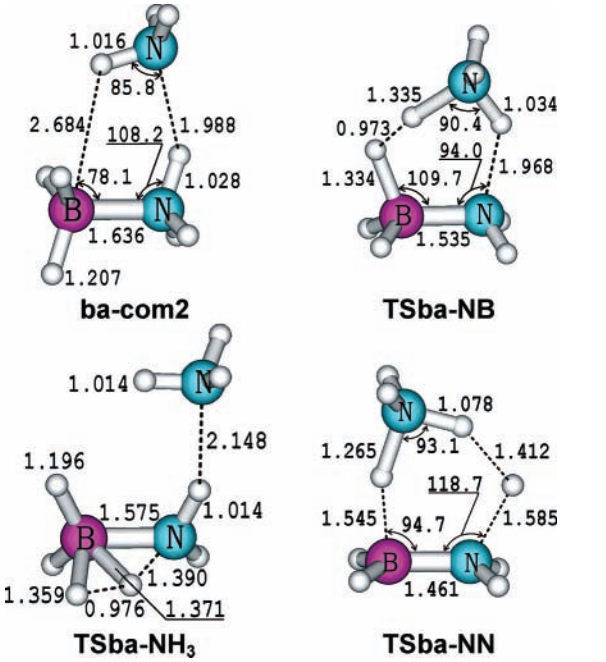

Figure 10. Geometrical parameters of the points for the $BH_3NH_3 + NH_3$ reaction: initial complex **ba-com2** and transition state structures **TSba-NB**, **TSba-NH**, and **TSba-NN** optimized from MP2/aVTZ calculations. Bond lengths are given in angstroms and bond angles in degrees.

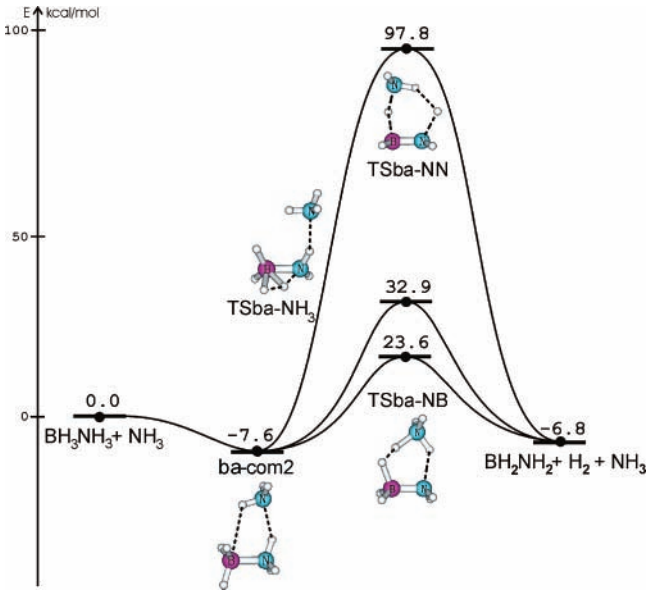

Figure 11. Schematic energy profiles showing the reaction pathways for H_2 release from BH_3NH_3 with NH_3 as the catalyst. Relative energies in kilocalories per mole were obtained from CCSD(T)/CBS calculations.

participate as a comparable catalyst. For the $BH_3NH_3 + NH_3$ reaction, we located a preassociation complex and three different transition state structures, whose selected MP2/aVTZ geometrical parameters are displayed in Figure 10. The corresponding potential energy profiles are illustrated in Figure 11. The shape and characteristics of the stationary points involving NH_3 are similar in many respects to those involving BH_3 discussed above.

The complex **ba-com2** is essentially a hydrogen-bonded N−H−N complex between two NH_3 entities, characterized by a N−H distance of 1.99 Å, and in part assisted by a weaker B−H−N interaction (as seen by a longer B−H bond of 2.68 Å). In this complex, NH_3 plays the role of a H-bond acceptor and borane amine a H-bond donor. The complexation energy of **ba-com2** is −7.6 kcal/mol. The transition state structure **TSba-NH$_3$** corresponds to **TSba-lew** described above, in which NH_3 now interacts with **TSba** of the monomer from outside of the four-member framework and by H-bonding. Again, NH_3 acts as a H-bond acceptor, with a somewhat longer N−H bond of 2.14 Å. If BH_3 is regarded as a Lewis acid, then ammonia behaves, in this sense, as a Lewis base catalyst. With respect to the separated reactants, the energy barrier involving **TSba-NH$_3$** is calculated to be 32.9 kcal/mol, which represents a reduction of 3.5 kcal/mol with respect to the energy barrier of 36.4 kcal/mol in the monomer via **TSba** (Figure 3). Such stabilization arises from a H-bond interaction between **TSba** and NH_3, which remains, however, smaller than that of −7.6 kcal/mol for complexation of borane amine, yielding **ba-com2**. As a consequence, the overall effect of H-bonding interaction by ammonia does not favor H_2 release.

As indicated by the notation, **TSba-NN** involves participation of NH_3 in the transition state structure creating a N−H−H−N framework. Due to an electrostatic repulsion between two positively charged H(N) atoms, this orientation results in an extremely high-energy structure **TSba-NN**, 97.8 kcal/mol above the separated reactants. This is even more destabilized than **TSba-BB,** where the H(B) atoms are, as expected, less polarized. For both cases, this type of interaction can be ruled out as a possible reaction mechanism.

The process via **TSba-NB**, implies direct participation of NH_3 as a bifunctional H-transfer but with a N−H−H−B framework, and this structure can thus be compared to **TSba-BN**. This is the lowest energy transition structure, with an energy barrier of 23.6 kcal/mol relative to the separated reactants and 31.2 kcal/mol with respect to the preassociation complex **ba-com2**. The lower well depth for **ba-com2** leads to a barrier height of 31.2 kcal/mol from **ba-com2**, which is above the value of 23.9 kcal/mol for the BH_3 catalyst value going from **ba-com1** to **TSba-BN** (Figure 7). The difference of 7.3 kcal/mol in the energy barriers results in a change of several orders of magnitude in the corresponding rate coefficients. Our values for the unimolecular reaction, calculated by RRKM, are $k(298\ \mathrm{K}) = 2.2 \times 10^{-11}\ \mathrm{s}^{-1}$ and $k(373\ \mathrm{K}) = 5.0 \times 10^{-7}\ \mathrm{s}^{-1}$ for both 1 and 11 atm; this behavior is similar to that for the BH_3-catalyzed reaction in which the high-pressure limit is reached at 1 atm. In addition, very similar values are found for the TST results: $k_\infty(\mathrm{TST}, 298\ \mathrm{K}) = 1.8 \times 10^{-11}\ \mathrm{s}^{-1}$ and $k_\infty(\mathrm{TST}, 373\ \mathrm{K}) = 6.0 \times 10^{-7}\ \mathrm{s}^{-1}$. For the bimolecular reaction we obtained $k(298\ \mathrm{K}) = 1.8 \times 10^{-6}\ \mathrm{cm}^3\ \mathrm{molecule}^{-1}\ \mathrm{s}^{-1}$ and $k(373\ \mathrm{K}) = 6.9 \times 10^{-3}\ \mathrm{cm}^3\ \mathrm{molecule}^{-1}\ \mathrm{s}^{-1}$. All these values include ST tunneling correction; for no-tunneling and Wigner-corrected values, see Table 3. At 298 and 373 K the tunneling factors are similar for both eqs 8 and 9: $Q_{\mathrm{tunnel,W}}(298\ \mathrm{K}) = 1.54$ versus $Q_{\mathrm{tunnel,ST}}(298\ \mathrm{K}) = 2.67$, and $Q_{\mathrm{tunnel,W}}(373\ \mathrm{K}) = 1.35$ versus $Q_{\mathrm{tunnel,ST}}(373\ \mathrm{K}) = 1.77$. In summary, the catalytic effect of BH_3 is substantially larger than that of NH_3.

At 373 K, we estimate the potential for production of H_2 as the formation of BH_3 from cleavage of the B−N bond in BH_3-NH_3 as this is the rate-determining step by a factor of $>10^6$ if the BH_3 is not trapped in a complex. If a complex is formed at higher pressures and all of the energy is dissipated, then the rate-determining step would be the BH_3 catalytic reaction, which is about 6 times slower than BH_3 formation. In any case, the slowest rate would be on the order of $0.1-1\ \mathrm{s}^{-1}$. Thus, with BH_3 as the catalyst, H_2 release could readily occur under mild conditions, consistent with the calorimetric experiments of the

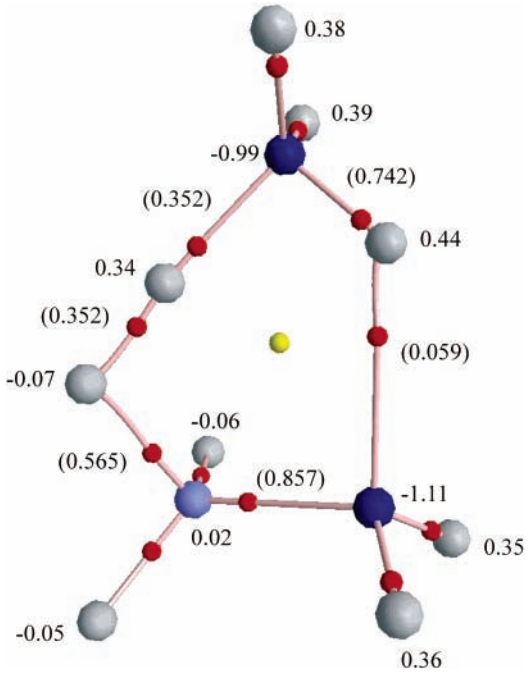

Figure 12. Molecular graph of transition state structure **TSba-NB** (red, bond critical points; dark blue, carbon atom; gray, hydrogen atoms; violet, boron). NBO charges were from B3LYP/6-311++G(d,p) calculations. Bond orders are shown in parentheses.

thermal decomposition of BH_3NH_3 below its melting temperature of 385 K by Wolf et al.[5b]

Electronic Reorganization along Different H_2 Elimination Processes. To obtain additional insight into the electronic mechanism of the catalysis, the molecular graphs generated on the basis of the electron densities constructed at the B3LYP/6-311++G(d,p) level in the different transition structures were analyzed; see Figures 8 and 12. An interesting feature in the corresponding transition structure is the appearance of a type of B−H−H−X dihydrogen interaction (X = C, N).[34] In many aspects, the electronic reorganization of ethane and borane amine are qualitatively similar.

The calculated NBO charges (Figure 8a) for **TSba** show a large negative charge of −1.06 e on the N-atom, with the B being almost neutral, −0.01 e. The H-atoms in the immediate vicinity of nitrogen are positively charged, >0.35 e.

In the most important structure, **TSba-BN**, BH_3 makes a dihydrogen bond, B−H−H−N, six-membered ring formation is effectively observed, and this is characterized by the presence of a ring critical point (Figure 8b). Calculated NBO charges suggest a negative charge of magnitude of −1.07 e on N, similar to that in **TSba**. In **TSba-BN**, the B-atom in the borane amine has a positive charge, 0.33 e, whereas the additional BH_3 boron atom bears a negative charge of magnitude −0.24 e. An ELF analysis shows the existence of a trisynaptic basin [*V*(H,B,B)] in this transition state structure, as illustrated in Figure 13. A qualitative explanation for the energetic favorability of **TSba-BN** can be provided with the help of the NBO and ELF data. A stabilizing electrostatic interaction between the positively charged H−H unit, under formation, with the rest of the molecule, in particular with the two negatively charged B and N ends within the B−H−H−N framework, is larger in **TSba-BN**. We can see in Figure 8b that the B−H−H−N framework shows a practically linear N−H−H arrangement, in contrast with that of the B−H−H, which is bent. This geometrical arrangement is in agreement with solid state analysis performed by Klooster et al.,[43] although the H···H distance is short in **TSba-BN**, close to that of 0.74 Å in H_2 (0.89 Å versus 2.02 Å in the crystal structure). The more polar N(δ^-)−H(δ^+) subunit tends to facilitate the H atom departure and, in the meantime, stabilizes the forming H_2 entity. The atom arrangement in the transition structure allows a hydrogen abstraction by the BH_3 boron and a simultaneous B−H bond cleavage and H−H bond formation. If it is assumed that the incoming BH_3 unit is sp^2-hybridized, the hydrogen abstraction is facilitated by the vacant p-orbital perpendicular to the BH_3 plane. The interaction of the vacant orbital with a negatively charged BH hydrogen atom of **TSba-BN** is expected to be more favorable as compared to the interaction of the vacant orbital with the positively charged NH hydrogen atom in **TSba-BB**. The optimized geometry shows that **TSba-BN** has a BH_4 subunit. The NBO charges indicate that the (B,H,H,H) group around borane bears a negative charge of −0.23 e, leading to some contribution from the [BH_4^-]-[$NH_3BH_2^+$] resonance structure, consistent with the fact that the $NH_3BH_2^+$ cation is the most stable protonated form of BH_2-NH_2.

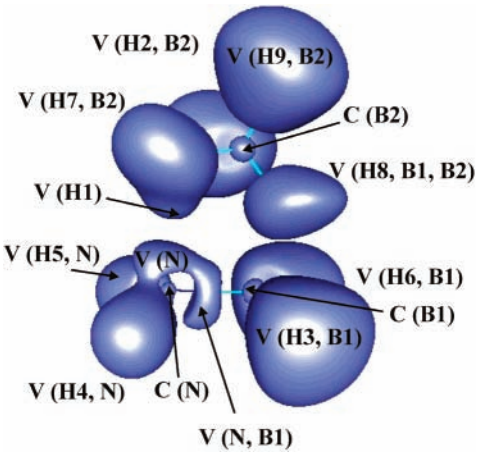

Figure 13. ELF isosurfaces ($\eta = 0.8$) of the catalyzed transition state structure for H_2 release **TSba-BN**.

Conclusion

We have located reaction pathways using state-of-the-art quantum chemical methods and analyzed the electronic reorganization during H_2 release in ethane and borane amine. We have identified the role of BH_3 and NH_3 fragments produced by decomposition of the B−N bond in BH_3NH_3, in particular BH_3, as an active bifunctional acid−base catalyst for H_2 formation. For ethane, the barrier height for H_2 production is reduced by more than 50 kcal/mol with BH_3 as the catalyst. For borane amine, we were able to locate six different transition structures for the H_2 dissociation with either an additional BH_3 or NH_3 present. Together with a more conventional pathway where the BH_3 behaves as a Lewis acid catalyst, we find an energetically low-lying reaction channel involving participation of BH_3 as a catalyst, which actively participates in the hydrogen transfer through a six-membered cyclic transition structure involving a B−H−H−N interaction. NH_3 shows similar behavior but with less capability to reduce the barrier height. Stabilizing electrostatic interactions are likely the main reason for the beneficial catalytic effect of BH_3. The barrier height in the catalytic pathway for H_2 release from borane amine with BH_3 as the catalyst is 6.1 kcal/mol with respect to the separated reactants and 23.9 kcal/mol from the complex BH_3NH_3···BH_3. The former corresponds to a reduction of 30 kcal/mol, relative to that of the monomer, and is consistent with the experimental findings[5] that the H_2 release from borane amine proceeds under

mild conditions below the melting temperature of 385 K. In summary, our present calculations demonstrate that in either ethane or borane amine, 1,2-H_2 release is greatly accelerated by the active participation of a BH_3 molecule. The BH_3 acts as a bifunctional (acid−base) catalyst facilitating H-transfer leading to H_2 bond formation. For a viable chemical hydrogen storage system, one must not only have good thermodynamics and good kinetics for release of H_2 but one must also have a cost-effective process to regenerate the original chemical hydrogen storage system from the depleted material. Studies of hydrogen regeneration processes are ongoing in our laboratory as well as in a number of other laboratories focused on chemical hydrogen storage. The chemistry involved in the regeneration process is likely to be quite different from that for H_2 release.

Acknowledgment. We thank Professor D. Truhlar for helpful comments on the effects of tunneling in chemical reactions. Funding was provided in part by the Department of Energy, Office of Energy Efficiency and Renewable Energy under the Hydrogen Storage Grand Challenge, Solicitation DE-PS36-03GO93013. This work was done as part of the Chemical Hydrogen Storage Center. D.A.D. is indebted to the Robert Ramsay Endowment of the University of Alabama. The Leuven group thanks the KULeuven Reseach Council (GOA program), FWO-Vlaanderen, and Belgian Technology Cooperation (BTC) for support.

Supporting Information Available: Tables of optimized geometries (Cartesian coordinates), calculated total MP2 and CCSD(T) energies (E_h) as a function of basis set with the CCSD-(T) values extrapolated to the complete basis set limit, calculated zero-point energy corrections, and tunneling corrections and figures showing normal coordinates associated with the imaginary frequencies in **TSet** and **TSet-b**, dissociation path for breaking the B−N bond in BH_3NH_3, molecular graph of transition structure **TSet-b** with NBO charges, and normal coordinates associated with the imaginary frequencies in **TSba**, **TSba-BN**, and **TSba-NB**. This material is available free of charge via the Internet at http://pubs.acs.org.

References and Notes

(1) (a) *Basic Energy Needs for the Hydrogen Economy*; Dressalhaus, M., Crabtree, G., Buchanan, M., Eds.; Basic Energy Sciences, Office of Science, U.S. Department of Energy: Washington, DC, 2003. (b) Maelund, A. J.; Hauback, B. C. In *Advanced Materials for the Energy Conversion II*; Chandra, D., Bautista, R. G., Schlapbach, L., Eds.; The Minerals, Metals and Materials Society: Warrendale, PA, 2004.

(2) Parry, R. W.; Schultz, D. R.; Girardot, P. R. *J. Am. Chem. Soc.* **1958**, *80*, 1.

(3) Sorokin, V. P.; Vesnina, B. I.; Klimova, N. S. *Russ. J. Inorg. Chem.* **1963**, *8*, 32.

(4) (a) Geanangel, R. A.; Wendlandt, W. W. *Thermochim. Acta* **1985**, *86*, 375. (b) Sit, V.; Geanangel, R. A.; Wendlandt, W. W. *Thermochim. Acta* **1987**, *113*, 379. (c) Wang, J. S.; Geanangel, R. A. *Inorg. Chim. Acta* **1988**, *148*, 185.

(5) (a) Wolf, G.; van Miltenburg, R. A.; Wolf, U. *Thermochim. Acta* **1998**, *317*, 111. (b) Wolf, G.; Baumann, J.; Baitalow, F.; Hoffmann, F. P. *Thermochim. Acta* **2000**, *343*, 19. (c) Baitalow, F.; Baumann, J.; Wolf, G.; Jaenicke-Rlobler, K.; Leitner, G. *Thermochim. Acta* **2002**, *391*, 159.

(6) (a) Dixon, D. A.; Gutowski, M. *J. Phys. Chem. A* **2005**, *109*, 5129. (b) Grant, D.; Dixon, D.A. *J. Phys. Chem. A* **2006**, *110*, 12955.

(7) Grant, D.; Dixon, D. A. *J. Phys. Chem. A* **2005**, *109*, 10138.

(8) (a) Li, Q. S.; Zhang, J.; Zhang, S. *Chem. Phys. Lett.* **2005**, *404*, 100. (b) Zhang, J.; Zhang, S.; Li, Q. S. *J. Mol. Struct. (THEOCHEM)* **2005**, *717*, 33.

(9) (a) Nguyen, M. T.; Ha, T. K. *J. Am. Chem. Soc.*, **1984**, *106*, 599. (b) Nguyen, M. T.; Hegarty, A. F. *J. Am. Chem. Soc.*, **1984**, *106*, 1552. (c) Nguyen, M. T.; Raspoet, G.; Vanquickenborne, L. G. *J. Am. Chem. Soc.* **1997**, *119*, 2552.

(10) Clark, T. J.; Russell, C. A.; Manners, I. *J. Am. Chem. Soc.* **2006**, *128*, 9582.

(11) Jaska, C. A.; Temple, K.; Lough, A. J.; Manners, I. *J. Am. Chem. Soc.* **2003**, *125*, 9424.

(12) Denney, M. C.; Pons, V.; Hebden, T. J.; Heinekey, D. M.; Goldberg, K. I. *J. Am. Chem. Soc.* **2006**, *128*, 12048.

(13) Stephens, F. H.; Baker, R. T.; Matus, M. H.; Grant, D. J.; Dixon, D. A. *Angew. Chem.* **2006** on line, early view, Nov. 28.

(14) Frisch, M. J.; Trucks, G. W.; Schlegel, H. B.; Scuseria, G. E.; Robb, M. A.; Cheeseman, J. R.; Montgomery, Jr., J. A.; Vreven, T.; Kudin, K. N.; Burant, J. C.; Millam, J. M.; Iyengar, S. S.; Tomasi, J.; Barone, V.; Mennucci, B.; Cossi, M.; Scalmani, G.; Rega, N.; Petersson, G. A.; Nakatsuji, H.; Hada, M.; Ehara, M.; Toyota, K.; Fukuda, R.; Hasegawa, J.; Ishida, M.; Nakajima, T.; Honda, Y.; Kitao, O.; Nakai, H.; Klene, M.; Li, X.; Knox, J. E.; Hratchian, H. P.; Cross, J. B.; Bakken, V.; Adamo, C.; Jaramillo, J.; Gomperts, R.; Stratmann, R. E.; Yazyev, O.; Austin, A. J.; Cammi, R.; Pomelli, C.; Ochterski, J. W.; Ayala, P. Y.; Morokuma, K.; Voth, G. A.; Salvador, P.; Dannenberg, J. J.; Zakrzewski, V. G.; Dapprich, S.; Daniels, A. D.; Strain, M. C.; Farkas, O.; Malick, D. K.; Rabuck, A. D.; Raghavachari, K.; Foresman, J. B.; Ortiz, J. V.; Cui, Q.; Baboul, A. G.; Clifford, S.; Cioslowski, J.; Stefanov, B. B.; Liu, G.; Liashenko, A.; Piskorz, P.; Komaromi, I.; Martin, R. L.; Fox, D. J.; Keith, T.; Al-Laham, M. A.; Peng, C. Y.; Nanayakkara, A.; Challacombe, M.; Gill, P. M. W.; Johnson, B.; Chen, W.; Wong, M. W.; Gonzalez, C.; Pople, J. A. Gaussian 03, Revision C.01; Gaussian, Inc.: Wallingford CT, 2004.

(15) MOLPRO is a package of ab initio programs designed by H.-J.Werner and P. J. Knowles: Amos, R. D.; Bernhardsson, A.; Berning, A.; Celani, P.; Cooper, D. L.; Deegan, M. J. O.; Dobbyn, A. J.; Eckert, F.; Hampel, C.; Hetzer, G.; Knowles, P. J.; Korona, T.; Lindh, R.; Lloyd, A. W.; McNicholas, S. J.; Manby, F. R.; Meyer, W.; Mura, M. E.; Nicklass, A.; Palmieri, P.; Pitzer, R.; Rauhut, G., Schütz, M.; Schumann, U.; Stoll, H., Stone, A. J.; Tarroni, R.; Thorsteinsson, T.; Werner, H.-J. MOLPRO, version 2002.6.

(16) (a) Becke, A. D. *J. Chem. Phys.*, **1993**, *98*, 5648. (b) C. Lee, C.; Yang, W.; Parr, R. G. *Phys. Rev. B* **1988**, *37*, 785.

(17) Gonzalez, C.; Schlegel, H. B. *J. Chem. Phys.* **1989**, *90*, 2154.

(18) Pople, J. A.; Seeger, R.; Krishnan, R. *Int. J. Quant. Chem. Chem. Symp.* **1977**, *11*, 149.

(19) (a) Cizek, J. *Adv. Chem. Phys.* **1969**, *14*, 35. (b) Purvis, G. D.; Bartlett, R. J. *J. Chem. Phys.*, **1982**, *76*, 1910. (c) Pople, J. A.; Head-Gordon, M.; Raghavachari, K. *J. Chem. Phys.*, **1987**, *87*, 5968.

(20) (a) Dunning, T. H., Jr. *J. Chem. Phys.* **1989**, *90*, 1007. (b) Kendall, R. A.; Dunning, T. H., Jr.; Harrison, R. J. *J. Chem. Phys.* **1992**, *96*, 6796.

(21) Peterson, K. A.; Woon, D. E.; Dunning, T. H., Jr. *J. Chem. Phys.* **1994**, *100*, 7410.

(22) Rittby, M.; Bartlett, R. J. *J. Phys. Chem.* **1988**, *92*, 3033.

(23) Knowles, P. J.; Hampel, C.; Werner, H.-−J. *J. Chem. Phys.* **1994**, *99*, 5219.

(24) Deegan, M. J. O.; Knowles, P. J. *Chem. Phys. Lett.* **1994**, *227*, 321.

(25) Peterson, K. A.; Dunning, T. H., Jr. *J. Chem. Phys.* **2002**, *117*, 10548.

(26) Davidson, E. R.; Ishikawa, Y.; Malli, G. L. *Chem. Phys. Lett.* **1981**, *84*, 226.

(27) Moore, C. E. *Atomic energy levels as derived from the analysis of optical spectra, Volume 1, H to V*; U.S. National Bureau of Standards Circular 467, COM-72-50282; U.S. Department of Commerce, National Technical Information Service: Washington, DC, 1949.

(28) (a) Bader, R. F. W. *Atoms in Molecules, A Quantum Theory*; Oxford University Press: Oxford, U.K., 1995. (b) Popelier, P. *Atoms in Molecules, An Introduction*; Prentice Hall: Englewood Cliffs, NJ, 2000.

(29) (a) Becke, A. D.; Edgekombe, K. E. *J. Chem. Phys.* **1990**, *92*, 5397. (b) Silvi, B.; Savin, A. *Nature* **1994**, *371*, 683.

(30) Reed, A. E.; Curtiss, L. A.; Weinhold, F. *Chem. Rev.* **1988**, *88*, 899.

(31) (a) Sander, S. P.; Friedl, R. R.; Ravishankara, A. R.; Golden, D. M.; Kolb, C. E.; Kurylo, M. J.; Huie, R. E.; Orkin, V. L.; Molina, M. J.; Moortgat, G. K.; Finlayson-Pitts, B. J. *Chemical Kinetics and Photochemical Data for Use in Atmospheric Studies: Evaluation Number 14*; JPL Publication 02-25, National Aeronautics and Space Administration, Jet Propulsion Laboratory, California Institute of Technology: Pasadena, CA, 2003; http://jpldataeval.jpl.nasa.gov/pdf/JPL_02-25._rev02.pdf. (b) Frenkel, M.; Kabo, G. J.; Marsh, K. N.; Roganov, G. N.; Wilhoit, R. C. *Thermodynamics of organic compounds in the gas state, Vol. I*; Thermodynamics Research Center: College Station, TX, 1994.

(32) Silver, D. M.; Stevens, R. M. *J. Chem. Phys.* **1973**, *59*, 3378 and references therein.

(33) Schuurman, M. S.; Allen, W. D.; Schleyer, P. v. R.; Schaefer, H. F., III. *J. Chem. Phys.* **2005**, *122*, 104302.

(34) Custelcean, R.; Kackson, J. E. *Chem. Rev.* **2001**, *101*, 1963.

(35) Holbrook, K. A.; Pilling, M. J.; Robertson, S. H. *Unimolecular Reactions*, 2nd ed.; Wiley: Chichester, U.K., 1996.

(36) KHIMERA, Version 3.2: A software tool for calculations of chemical reactions thermodynamics and kinetics from first principles; Kintech, Kinetic Technologies, Ltd.: Moscow, 2003; http://www.kintech.ru/.

(37) Steinfeld, J. I.; Francisco, J. S.; Hase, W. L. *Chemical Kinetics and Dynamics*, 2nd ed.; Prentice Hall: Englewood Cliffs, NJ, 1999.

(38) (a) Kreevoy, M. M; Truhlar, D. G. *In Transition State Theory in Investigations of Rates and Mechanisms of Reactions*, 4th ed.; Bernasconi, C. F., Ed.; Wiley: New York, 1986; Part 1, p 13. (b) Johnston, H. S. *Gas Phase Reaction Rate Theory*; Ronald Press: New York, 1966. (c) Glasstone, S.; Laidler, K. J.; Eyring, H., *The Theory of Rate Processes*; McGraw-Hill: New York, 1941. (d) Garrett, B. C.; Truhlar, D. G. In *Encyclopedia of Computational Chemistry*; Schleyer, P. v. R., Allinger, N. L., Clark, T., Gasteiger, J., Kollman, P. A., Schaefer, H. F., III, Eds.; John Wiley & Sons: Chichester, U.K., 1998; p 3094.

(39) Wigner, E. Z. *Z. Phys. Chem. B* **1932**, *19*, 203.

(40) Skodje, R. T.; Truhlar, D. J. *J. Chem. Phys.* **1981**, *85*, 624.

(41) Zuev, P. S.; Sheridan, R. S.; Albu, T. V.; Truhlar, D. G.; Hrovat, D. A.; Borden, W. T. *Science* **2003**, *299*, 867.

(42) Patwari, G. N. *J. Phys. Chem. A* **2005**, *109*, 2035.

(43) Klooster, W. T.; Koetzle, T. F.; Siegbahn, P. E. M.; Richardson, T. B.; Crabtree, R. H. *J. Am. Chem. Soc.* **1999**, *121*, 6337.